Chapter

Changes in Arctic Ocean Climate Evinced through Analysis of IPY 2007–2008 Oceanographic Observations

J.N. Stroh, S. Kirillov, G. Panteleev, O. Francis, M. Yaremchuk, E. Bloshkina and N. Lebedev

Abstract

Full-depth hydrographical surveys conducted in 2007–2009 during the International Polar Year (IPY) collaboration provide an accurate snapshot of the Arctic Ocean (AO) hydrography at a time when the Arctic Ocean Oscillation (AOO) index was highest in recent record. We construct pan-Arctic temperature and salinity (T/S) reference states from these data using variational optimal interpolation and discuss some key differences between the 2007–2009 state and a similarly constructed climatology from historical 1950–1994 Russian archives. These data provide a recent, known reference state for both qualitative and quantitative future AO climate change studies. Furthermore, we present an analysis of sea-surface height (SSH) and upper-layer circulation constructed from the IPY data via 4DVar data assimilation and use them to examine circulation and freshwater source changes visible during IPY.

Keywords: Arctic Ocean climate, Arctic Ocean observations, data assimilation, gridded IPY climatology

1. Introduction

During the International Polar Year (IPY) 2007–2008, the international scientific community completed an intensive physical survey of the Arctic Ocean (AO). Many countries and institutions contributed to this effort, which generated a significant number of in situ hydrographical observations including stationary full-depth profiles of temperature/salinity (T/S) from conductivity-temperature-depth instruments (CTD) and partial-depth profiles of the upper ~700 m along Lagrangian tracks followed by Ice-Tethered Profiler (ITP) affixed to sea ice, measurements of T/S along the tracks followed by submarine gliders near coastal areas, and a small number of profiles from less accurate expendable CTD and expendable bathythermograph (XBT) instruments.

Arctic T/S distribution is governed largely by water inflow and outflow through the major gateways, the properties of those waters, and regional circulation. AO sources include the warm saline waters advected with the Norwegian current from

North Atlantic [1], the fresh (relative to mean AO salinity) Pacific waters (PW) entering through Bering Strait [2], and the summertime fresh and warm river discharge from the Siberian and North American rivers [3, 4]. AO export occurs primarily through Fram Strait by way of the Transpolar and East Greenland currents and also through less-studied Canadian Archipelago transport [5]. Within the AO, shelf-basin exchanges are typically restricted to bathymetric features, such as Herald and Barrow Canyons in the Chukchi Sea [6] and St. Anna Trough north of Severnaya Zemlya in the Kara Sea [7]. Regional circulation is governed by topographically steered boundary currents along shelf breaks and other topographic features, restricted by density fronts between water masses of disparate origin, and subjected to external forcing including surface heating (cooling) in summer (winter) with significant effects from sea-ice melt/freeze and large-scale atmospheric pressure systems [1, 8–10].

The IPY effort occurred at a significant time, coincidental with the largest recent positive Arctic Ocean Oscillation (AOO) index, a measure derived. From the central AO sea-surface height gradient over the central AO, which indicates strength of large-scale anticyclonic flow [11]. Prior to IPY, the AOO index had been in an overall positive regime for nearly two decades, while historical records suggest a sub-decadal frequency [9] (updated at www.whoi.edu/page/preview.do?pid=66578). Other modes of regional oscillation occur with timescales of 60–80 years [12]. At the same time, in summer 2007, winds associated with the Beaufort High remained predominantly anticyclonic—a feature common to the Arctic winter but unusual for summer [13]—so Beaufort Gyre (BG) sea-level response to atmospheric forcing strengthened the AOO. Additionally, 2007 was a monumental year for river discharge; Eurasian river discharge surpassed the 2002 record by nearly 10% [14]. The effects of these drivers, whether purely anomalous or the result of long-term variability, relate to pronounced recent changes in the Arctic marine climate system and were witnessed by the IPY survey efforts.

Over a decade has passed since many of the observed strong and rapid warming trends were confirmed as both present and underway. Older climatologies may be inadequate for the study of more recent changes as they may depend much on pre-1996 data when the positive AOO regime was not such a strong and permanent feature of the region, thicker and more extensive sea ice regulated mechanical and thermodynamical fluxes with the atmosphere, continental riverine discharge was less, and the Lomonosov Ridge roughly defined a partition of the Arctic between Atlantic and Pacific upper-ocean layers. The thermal state of the AO over the past decade is above the long-term average, and this warming greatly affects both hydrographic and ice-related processes observed in the high latitudes; changes occurring under these new conditions are of particular interest [5, 13, 15–23].

Unlike other oceans, vertical stratification of AO water masses is governed more by salinity than temperature, and density gradients readily allow for decomposition of profiles into differentiated, typically noninteractive layers. Away from regions of significant freshwater influence, the vertical distribution of water masses throughout the AO generally comprises a well-mixed surface layer occupying the upper 50–100 m, underlain by a layer of intermediate water of Pacific origin (absent in the eastern, Atlantic domain of the Arctic), followed by a layer of warmer more saline water of Atlantic origins and an Arctic deepwater bottom layer. Importantly, the halocline of Pacific-originated waters overlies the warmer Atlantic water in the ocean in the Pacific sector [24], buffering sea ice from the warmer Atlantic waters below. The presence, thickness, and specific properties of each layer vary laterally throughout the Arctic [10, 25], and one may distinguish between layers of waters of Pacific and Atlantic origin on the depth of local haloclines and isotherms characteristic within each column.

The remote nature of the AO, together with practical difficulties in observation and navigation due to sea ice and sparse infrastructure, makes in situ sampling of the AO expensive and occasional. Satellite monitoring of the ocean surface is possible but inhibited by ice cover and clouds. Unfortunately, the accuracy of the satellite-surface observations and their processed (i.e., L2–L4) products is often far from optimal: they may contain large errors due to poor calibration, mask large portions of the AO for sea ice and thus lack of coverage over the central AO, and may contain anachronistic assumptions in their post-processing algorithms [26]. Modeling efforts and other interdisciplinary studies in need of static background ocean data may need to rely on gridded products that are biased toward older AO regimes or large amounts of surface observations from satellite. Further, climatological studies using older reference states for trend analysis may suffer from amplified trend errors. For example, the Arctic portion of the most recently available Polar Science Center Hydrographic Climatology (PHC 3.0, updated from [27]) is based on historic observations through 1993 [28, dataset g01961].

The concerns listed above motivate this work, which presents a 2007–2009 AO stationary analysis state inferred from algorithmic data conditioning of pan-Arctic hydrographical surveys and other at-depth observations to provide a snapshot of the non-coastal ocean state with an emphasis on the intermediate layers. The result is a dataset of gridded T/S available in NetCDF at http://bit.ly/2M6qsJ9, from which this chapter discusses mapped water masses and their differences relative to those mapped from 1950 to 1994 climatology. We also use 4DVar data assimilation to establish an analysis of major circulation changes during IPY relative to the climatological mean and discuss the evident anomalies of July–December 2008 [29]. The remainder of this chapter is organized as follows: Section 2 discusses the in situ data and the production algorithm for the gridded fields, Section 3 presents an atlas of water mass properties for the IPY and their differences from historical data fields, Section 4 discusses changes in the AO water mass distribution and thermal state evident from the use of IPY data and derived climatology, Section 5 presents analysis of circulation anomalies during the IPY, and Section 6 concludes the chapter.

2. Observational data and gridding

As part of an IPY initiative, approximately 13,000 CTD/xCTD/XBT profiles along with ITP data were curated into a central database of AO T/S observations from contributors in Japan, Norway, Russia, Canada, the USA, Germany, Poland, Sweden, and China. Stroh et al. [[26], Figure 1] show the location of profiles over the AO, of which only the IPY CTD and ITP data during 2007–2008 are used here. CTD observations during the sea-ice minimum months of August–October account for approximately 40% of all ship-borne profiles, while wintertime November–March account for approximately 30%. ITP apparatuses provide a more temporally uniform stream of profile data for the uppermost ~700 m throughout the year; ITP data were collected and made available by the Ice-Tethered Profiler Program [30, 31] based at the Woods Hole Oceanographic Institution (http://www.whoi.edu/itp).

The Data-Interpolating Variational Analysis tool (DIVA, [32]) is a robust finite element-based optimization tool for gridding large 2D, 3D, and 4D datasets and includes error estimates of the analysis. This freely available program, developed by the GeoHydrodynamics and Environment Research, was applied to the observational data described above to construct static full-depth fields on an equal-area polar-centered grid with 50 km resolution. Interpolation to 51 vertical levels occurs level-wise within DIVA, to which an internally applied stability algorithm ensures that analyses remain hydrodynamically stable with respect to density throughout

the gridding. Bathymetric masking was inferred from the International Bathymetric Chart of the Arctic Ocean [33], and regions with depth less than 200 m are masked. The correlation length scales for observations correspond to three grid cells with a signal-to-noise ratio of 10%. The same procedure applied to historical observations collected during 1950–1994 (privately archived at the Arctic and Antarctic Research Institute of Russia) generates mean climate dataset for that period, which is used to contrast the gridded IPY data.

3. Water mass distribution maps

From the gridded T/S analyses for the 1950–1994 and IPY periods, water mass properties reveal qualitative differences between them. The use of density-related properties to distinguish water masses is less certain than chemical analysis [22, 34]. Scarcity of widespread chemical tracer surveys precludes such an approach here, and analysis based on the more common T/S data is adopted. This work chooses to map Atlantic water (AW) and summer Pacific water (SPW) for both their simplicity of definition and importance in the freshwater (FW) and thermal budget of the AO. Characteristics used to identify AW and SPW are adapted from [25] and [35, 36], respectively, and are described below.

The AW distinguishes an intermediate layer of warm water of Atlantic origin that has entered the Arctic Basin through deep coastal channels and bathymetric steering. Over-basin AW typically has $S \geq 34.8$ PSU with $T \geq 0°C$ despite heat loss along the Eurasian shelf. SPW denotes relatively fresh waters with 31 PSU $\leq S \leq 33$ PSU and $T \geq -1.4°C$ entering the AO through the Bering Strait which have cooled after residence on the shallow Chukchi Shelf and include substantial meteoric FW [21, 35]. These low-density waters form a subsurface layer in the western Arctic typically at depths between 50 and 100 m and often include a local temperature maximum [37, 38].

In **Figures 1–11**, left-side plots show the identified field for the IPY dataset, while the right-side plot shows the corresponding anomaly field relative to the

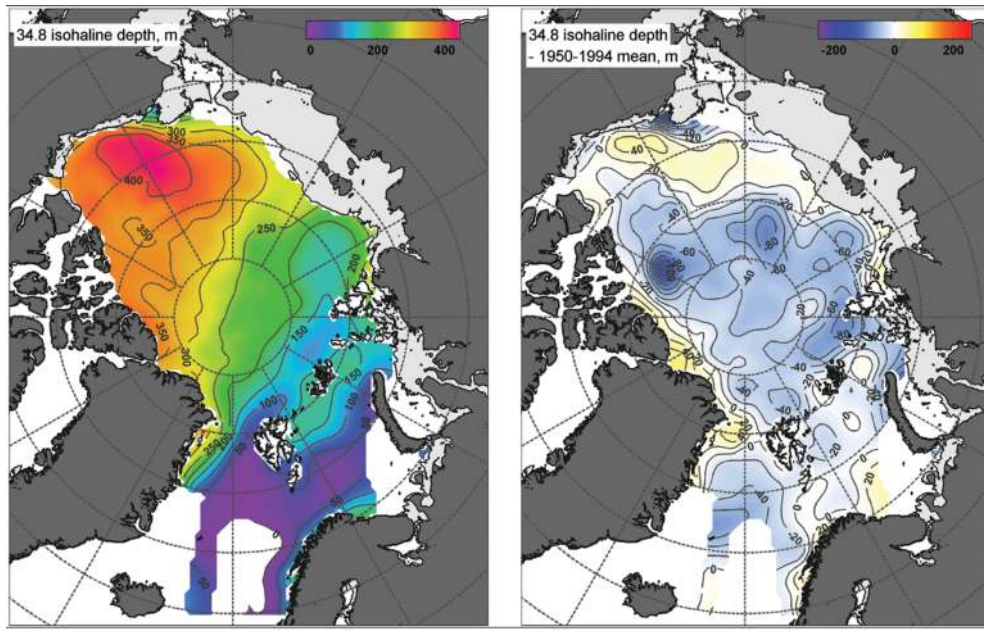

Figure 1.
34.8 PSU isohaline depth. IPY (l) and anomaly (r).

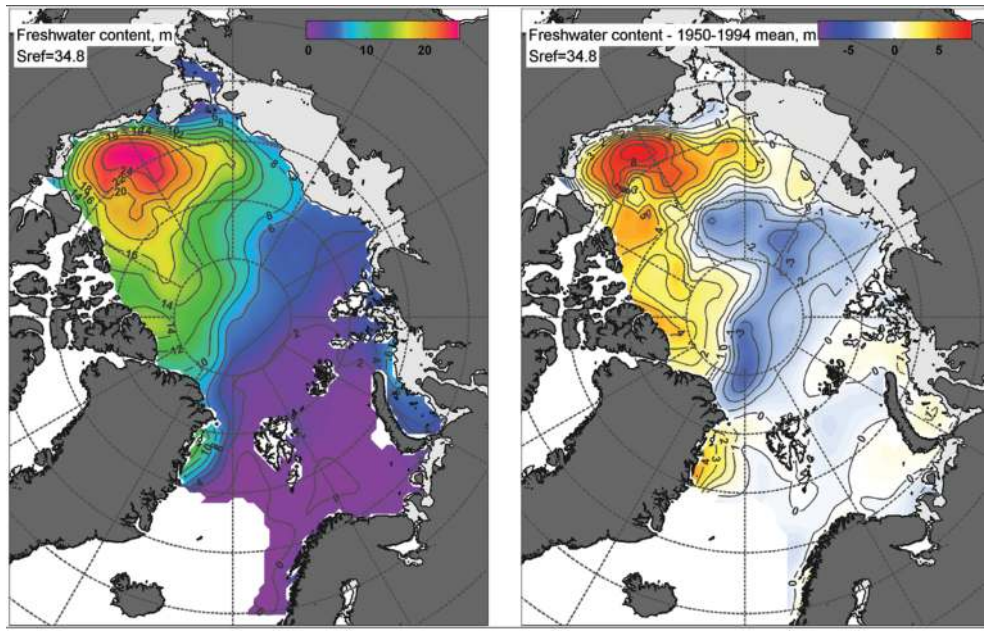

Figure 2.
FWC relative to 34.8 PSU isohaline. IPY (l) and anomaly (r).

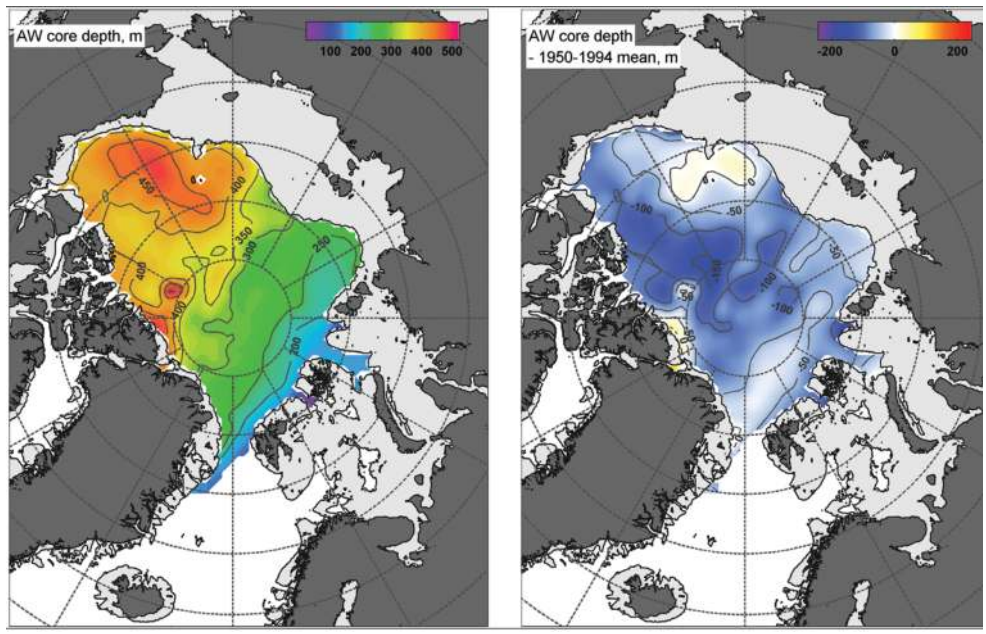

Figure 3.
AW core depth. IPY (l) and anomaly (r).

Russian 1950–1994 archive. We refer to each such pair singularly as a figure and distinguish between the field and its anomaly in context. **Figure 1** maps the 34.8 PSU isohaline depth. **Figure 2** shows the integrated FW content (FWC), in meters of freshwater, with respect to 34.8 PSU.

F**igures 3–7** plot the AW core depth, core temperature, heat content, lower boundary depth, and upper boundary depth, respectively. AW here is defined as waters composing a continuous vertical region of positive temperature bounded by 0°C isotherms, which define herein the lower and upper AW boundary depths. The AW core depth and temperature are adopted to be the depth and value of the

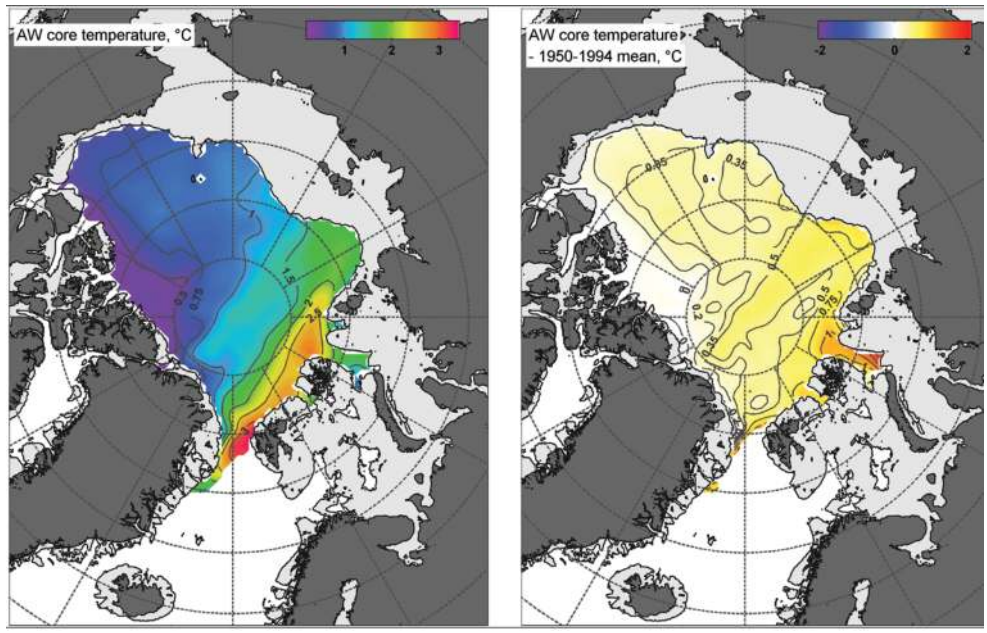

Figure 4.
AW core temperature. IPY (l) and anomaly (r).

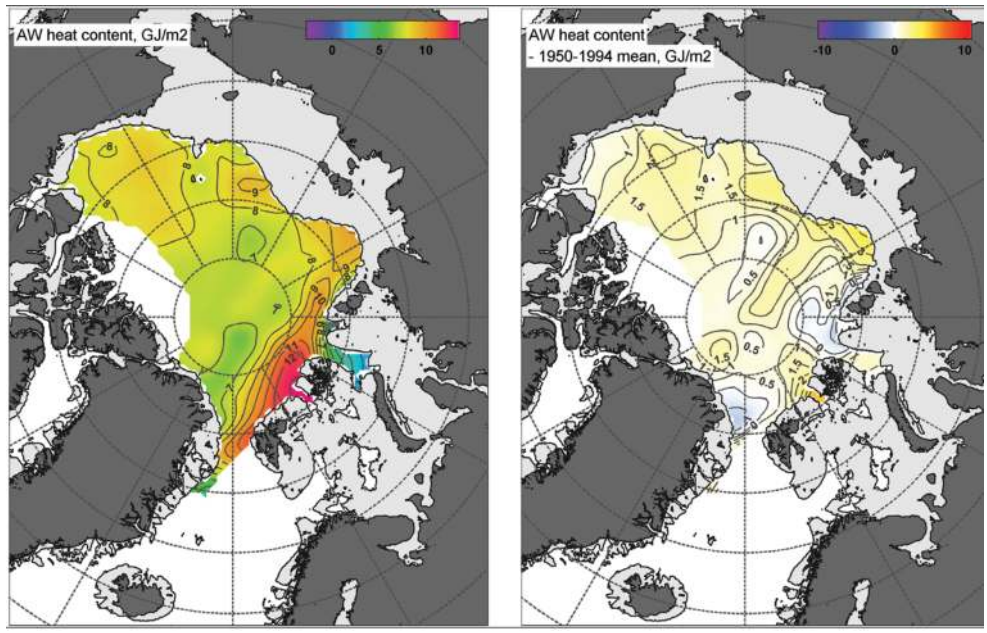

Figure 5.
AW heat content. IPY (l) and anomaly (r).

temperature maximum within the AW layer. Total heat content is calculated as the vertical integral of specific heat with respect to −1.8°C between AW boundaries.

Insufficient deep data in near the Canadian Archipelago precludes a resolution of the AW lower boundary and consequently of the heat content in that area.

Figures 8–11 show calculated fields for summer Pacific water, which exists only on the Pacific side of the Arctic. SPW is defined by a local temperature maximum

DOI: http://dx.doi.org/10.5772/intechopen.80926

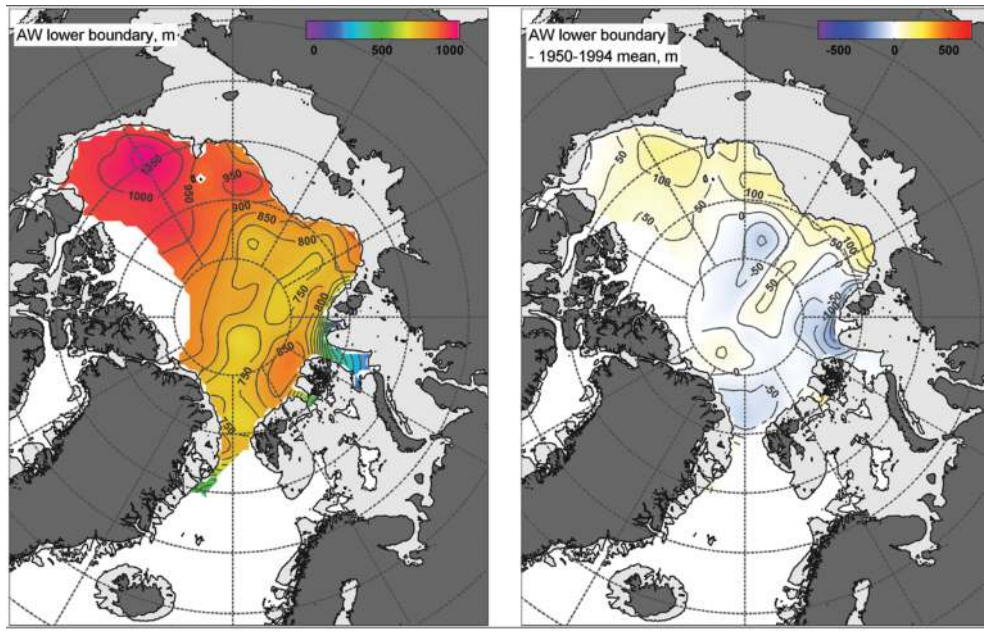

Figure 6.
AW lower boundary. IPY (l) and anomaly (r).

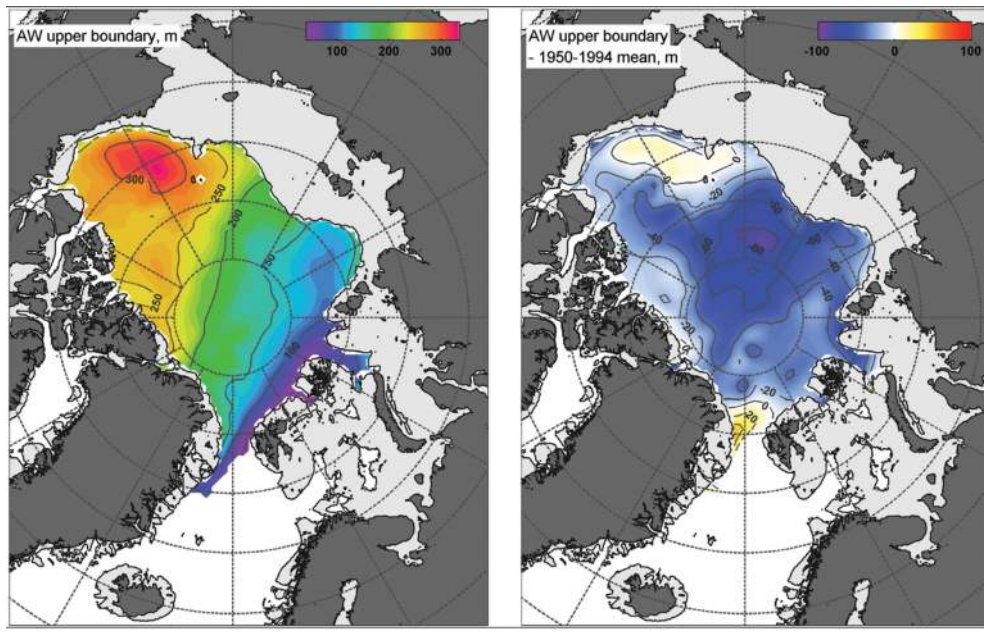

Figure 7.
AW upper boundary. IPY (l) and anomaly (r).

occurring below the surface mixed layer within the salinity range 30.5–33.0 PSU [35]. Upper and lower SPW boundary depths are determined $T \geq -1.4°C$ and salinity restriction to that range. **Figure 8** maps the depth of the maximum temperature found in SPW, and **Figure 9** identifies these maxima. **Figures 10** and **11** show the lower and upper boundary depths of SPW.

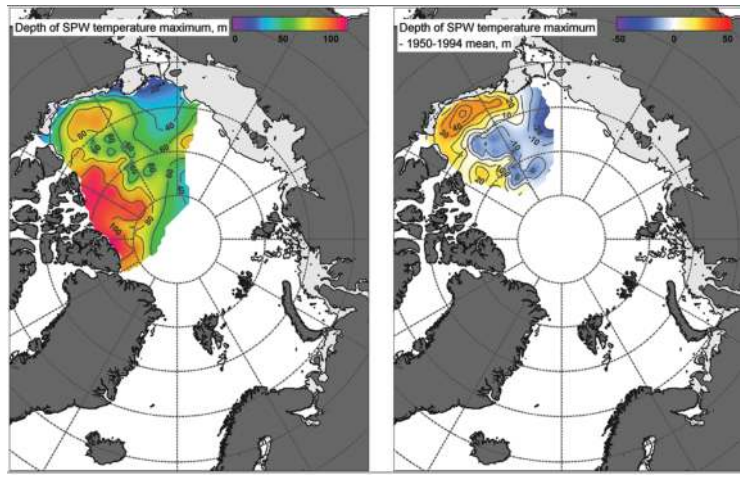

Figure 8.
Summer PW depth of T_{max}. IPY (l) and anomaly (r).

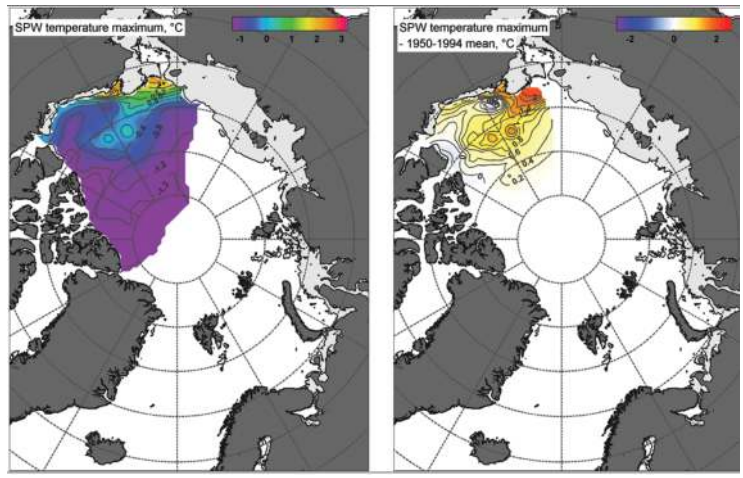

Figure 9.
Summer PW T_{max}. IPY (l) and anomaly (r).

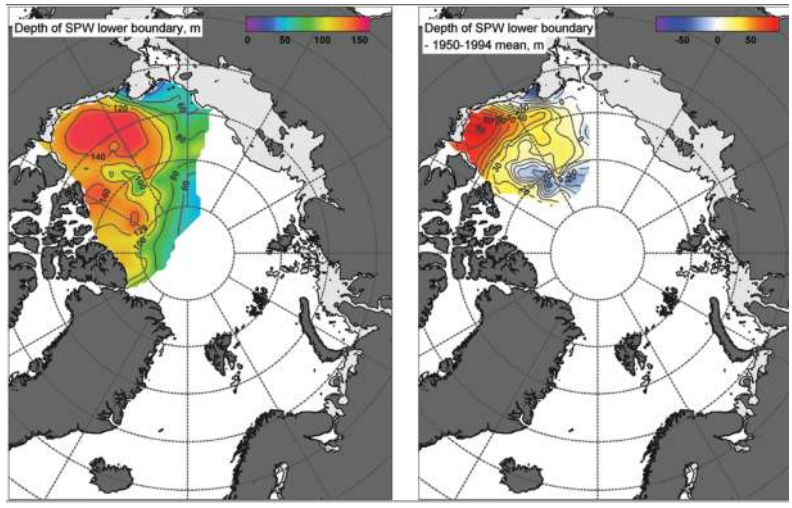

Figure 10.
Summer PW lower boundary depth. IPY (l) and anomaly (r).

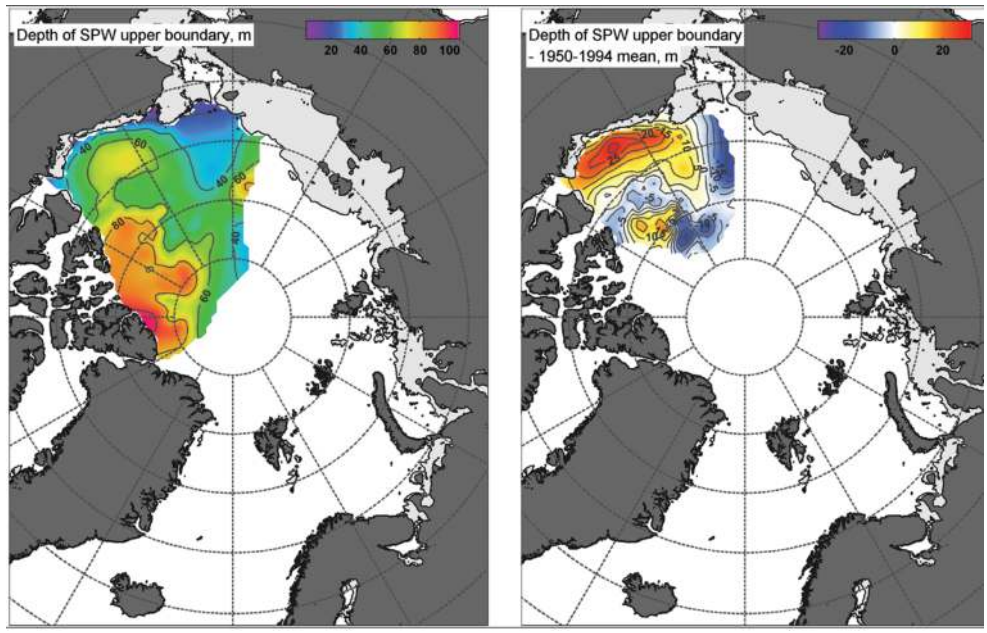

Figure 11.
Summer PW upper boundary depth. IPY (l) and anomaly (r).

4. Changes inferred from T/S observations

In general, the vertical and spatial patterns of hydrographic parameters in the AO and adjacent North Atlantic had undergone considerable changes by IPY although the large-scale distributions of the water masses align with the historic climatology. Readers unfamiliar with AO geography and its bathymetric features are encouraged to follow this discussion with an atlas, e.g. https://geology.com/articles/arctic-ocean-features/.

4.1 Atlantic waters

Elevated pan-Arctic heat content due to the extraordinary heat transported to the AO from the North Atlantic is a significant change evident during the IPY period. Advection of relatively warmer AW resulted in anomalous hydrographic state formation over the entire deep Arctic Basin [17, 38]. The temperatures within the core of AW were observed 0.3–1.0°C higher than climatic values; mean changes are ~0.65°C over the Eurasian Basin and ~0.25°C over Canada and Makarov basins.

Of further note is the warm tongue of AW that appears to be topographically steered by the Lomonosov Ridge; **Figure 4** shows a clear 0.5°C core temperature anomalous increase extending from the Laptev Sea toward the Greenland Shelf. This feature resides at a depth of about 275 m, ~75 m surfaceward of the historic AW core depth per **Figure 3**. Over the Makarov Basin, AW expanded ~50 m deep into the column [39], while the AW core depth has moved 100–150 m surfaceward with an associated 0.5–1.0 GJ/m^2 increase in associated heat content. Similar changes including the AW moving surfaceward and retaining more heat at depth are present throughout most of the AO indicating stronger potential influence on ice-related processes [40].

By 2007, the intermediate AW layer had deepened and thickened in the Pacific sector [23], but the changes are heterogeneous over the central and Eurasian basins.

In particular, the net AW layer thickness appears to have thinned over the Amundsen Basin, which is likely a mass-balance response to the thickened layer observed on the Pacific side of Lomonosov Ridge. Within the western side of Fram Strait, the AW layer has thickened by roughly 70 m, moving 20 m closer to the surface without change in the core depth.

4.2 Pacific water

Figure 2 shows another of the most drastic changes in the Arctic—the change in freshwater distribution. As a proxy for the AW-PW upper-ocean front in the central Arctic, the strong FW anomaly gradient illustrates the change from the Lomonosov Ridge to the Alpha-Mendeleev Ridge (AMR) system [22 and references therein, 41]. Further, the boundary marking the extent of present SPW in **Figures 9–11** tracks very directly the local bathymetric minimum of the AMR. Estimates shortly after IPY show that FWC in the Eurasian domain decreased by nearly one-quarter, while the American domain increased by the same percentage [16, 42]. The influx of PW through Bering Strait was near a record high in 2007, importing anomalously large FW volume and thermal input [20].

The loss of FWC near the pole and in the western sector likely results from cyclonic AO moving more AW toward the eastern Amerasian Basin. Simultaneously, the wind-forced anticyclonic BG stored fresher SPW in the Pacific sector, accumulating an average of 4 m FWC on the Pacific side of the front. Much of this FW had been in place prior to 2007; the IPY FWC in the Beaufort Sea is nearly identical to that found for 2006 [21]. Carmack et al. also find that sea-ice freeze/melt accounts for a net loss of FWC in the Beaufort Region, with riverine water and PW contributing roughly half of the regional FW [21]. Ge et al. find that the mean annual Yukon River outflow, the most significant meteoric source included in SPW, increased 8% between 1977 and 2006 [43].

An increasing trend in Eurasian catchment outflow also is evident [14] and related to changes in permafrost [44] and temporal changes in continental hydrological cycles [45]. Increased Siberian runoff suggests the apparent decreases in FW volumes adjacent to the Laptev and East Siberian seas arising from changes in seasonal ice and the regional dominance of AW, but these source changes alone do not explain FW accumulation observed in the Beaufort Sea during IPY and beyond [46]. Data-conditioned modeling of the 2008 circulation [29] suggests that this accumulation may be supported by transport from the Lincoln Sea [47] and/or regions north of Greenland.

Changes in the organization of water masses have also affected the outflow of AO through Fram Strait, located between Greenland and Svalbard. The Transpolar Drift mode arising from the cyclonic AOO regime impedes PW from reaching the continental shelf north of Greenland. Consequently PW may only exit the AO via the Canadian Archipelago [19], which has been shown to be a significant but variable route for AO export [5, 48, 49].

4.3 Directly observed from ITP data

The gridded IPY data do not resolve a surface layer. Sea-surface temperature and salinity (SST and SSS, respectively) are temporally variable as they depend on the strongly seasonal Arctic diurnal effects. Additionally SST/S in the AO depends seasonally on sea-ice-related processes such as meltwater strata, brine rejection, rapid wintertime heat loss through sea-ice leads, etc. Models and SST satellite data products often assume a surface freezing temperature (FT) of −1.8°C, which assumes background salinity of ∼32.86 PSU. At that T/S state, FT sensitivity is

DOI: http://dx.doi.org/10.5772/intechopen.80926

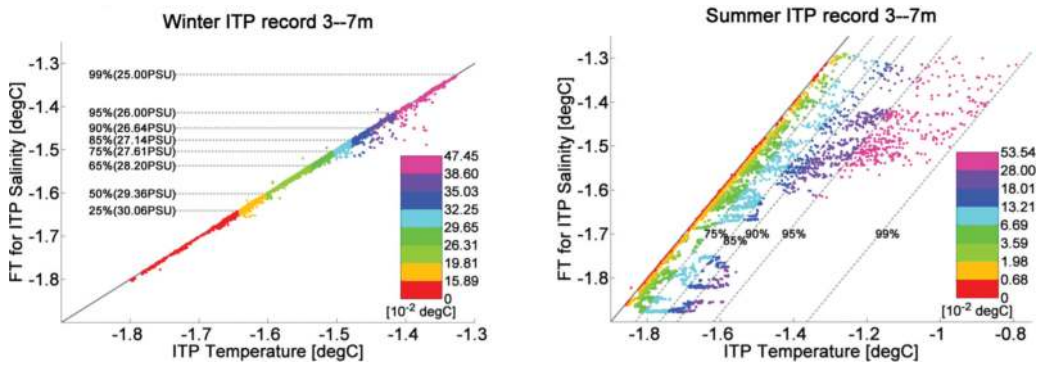

Figure 12.
Shallow ITP-observed temperature. Winter (l) and summer (r).

∼0.1°C per −0.01 PSU so that inaccuracies in background salinity amplify errors in associated freezing temperature.

Figure 12 illustrates the inaccuracies of these assumptions by examining the relationship between near-surface temperatures observed by 2006–2009 ITP and FT calculated from the associated salinity. Observations are primarily over the Pacific sector and central Arctic. The thick diagonal line shows exact correspondence between observed T and FT. Colors indicate binned values of T + 1.8°C (T-FT) in winter (summer) in the left (right) plot, with dashed lines demarcating percentiles as labeled. In winter months of November–April, all observations correspond to freezing point, but only about 25% of measurements have T ≤ −1.64°C, the freezing temperature associated with ∼30 PSU. In summer months of May–October, temperatures clearly depart from freezing, but only ∼25% of measurements differ from freezing by more than 0.05°C. In both summer and winter, the vertical structure of the plots demonstrates inaccuracy of the −1.8°C at ∼32.86 PSU assumption; surface waters in the western Arctic have salinities in the range 30–32 PSU.

5. Changes in circulation

5.1 Quasi-stationary "climatological" circulation

Freshwater changes throughout the Arctic relate to changes in geostrophic current distributions. Over basins, the strengthened FW gradient between the Pacific and Atlantic sectors led to a very significant sea-surface height (SSH) changes, which in turn gives rise to changes in geostrophic currents [16]. The strengthening of geostrophic currents in the Pacific sector is suspected among the factors for the reduction of multiyear ice over the Canadian Basin [50]. Other factors include deepening AW over the Canada Basin since 2004, enhancing the strength of the BG, and its accumulation of freshwater [23]. A recent study demonstrates that atmospheric modulation of geostrophic boundary currents and SSH quantifiably relates to the Northern Hemisphere annular mode strength [51].

To analyze the quantitative difference in the mean circulation during the IPY period with respect to the climatological circulation, the IPY dataset was conditioned using the four-dimensional variational (4DVar) data assimilation (DA) approach [52, 53] in two ways. To find a quasi-stationary solution, the process uses 4DVar optimization of an ocean model forced by the corresponding heat, salt, and momentum fluxes inferred from NCEP/NCAR reanalysis and regional Pan-Arctic Ice-Ocean Modeling and Assimilation System (PIOMAS). In the nonstationary reconstructions, all available T/S data were averaged for model grid bins, and these

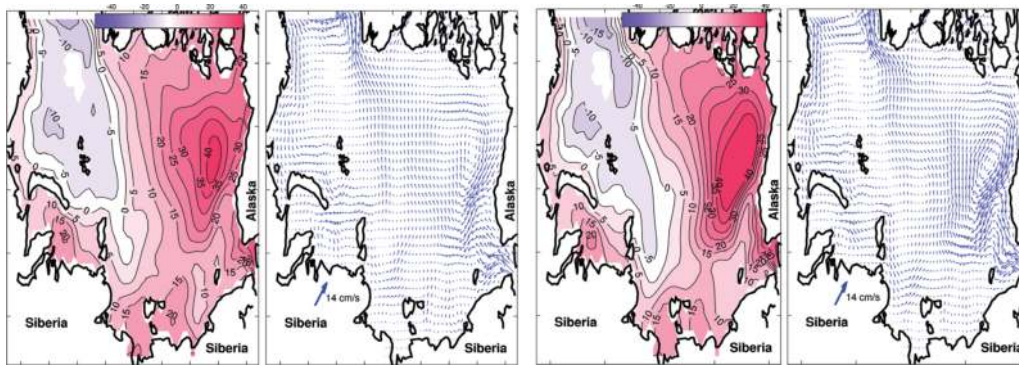

Figure 13.
Quasi-stationary model reconstruction of SSH and near-surface currents from historical 1900–2006 data (left plots) and the IPY data (right plots).

meaned observations were assimilated through the conventional 4DVar DA approach using a semi-implicit ocean model (SIOM) with resolution of 65 km; a framework of the algorithm is described in [52, 54].

The resulting quasi-stationary SSH maps and near-surface currents are shown in **Figure 13**. A comparison indicates the essential reorganization of the circulation in the AO evident during IPY. The most notable feature is the strong intensification and shift of the BG toward the Alaska. IPY SSH patterns are characterized by a pronounced BG dome which attains a central height greater than 50 cm, while the typical climatological SSH is only about 40 cm. This difference results from intensified westward flow along the Alaskan and Chukchi Sea continental slope. There is also a clear re-centering of the BG resulting from the shift of the Transpolar Drift axis toward the Canada Basin; this agrees well with the recent analysis of the freshwater content and circulations conducted by [55].

5.2 Anomalous 2008 circulation

The application of the more advanced 4DVar reconstruction of nonstationary circulation for July–December 2008 indicates stronger circulation than those directly detected from the in situ IPY dataset.

The SIOM-4DVar reconstructed bimonthly evolution of SSH and circulation at 250 m during July–December 2008 is shown in **Figure 14**. The SSH patterns are characterized by a pronounced BG dome which gets slightly stronger in November–December (**Figure 14**, right) attaining a 40 cm central elevation. Compared to the relatively smooth and symmetric SSH derived through optimal interpolation of observations (e.g., [16]), the DA-reconstructed SSH reveals finer features consistent with the observations. During September–October, the SSH pattern is characterized by a secondary SSH maximum at 74°N 140°W, which tends to erode by the end of the year but still persists as a tongue spreading toward Alaska along 140°W. This feature is seen in the AVISO anomalies averaged over the second half of 2008 [29].

Another prominent feature is a zonally spreading trough in the region between 72°N and 80°N from Severnaya Zemlya to the Bering Strait. The emergence of this depression could be one of the causes of intensification of the Bering Strait transport due to the increase of the large-scale sea level difference between the Chukchi and Bering Seas. This is supported by the analysis of Woodgate et al., who estimated the force balance controlling the flow through the Bering Strait and found a significant increase of the pressure head in 2007–2011 with respect to the 1997–2006 period when the Bering Strait transport was smaller [20 and Figure 1h therein]. The behavior of the SSH lowering is shown in the bimonthly SSH fields averaged over

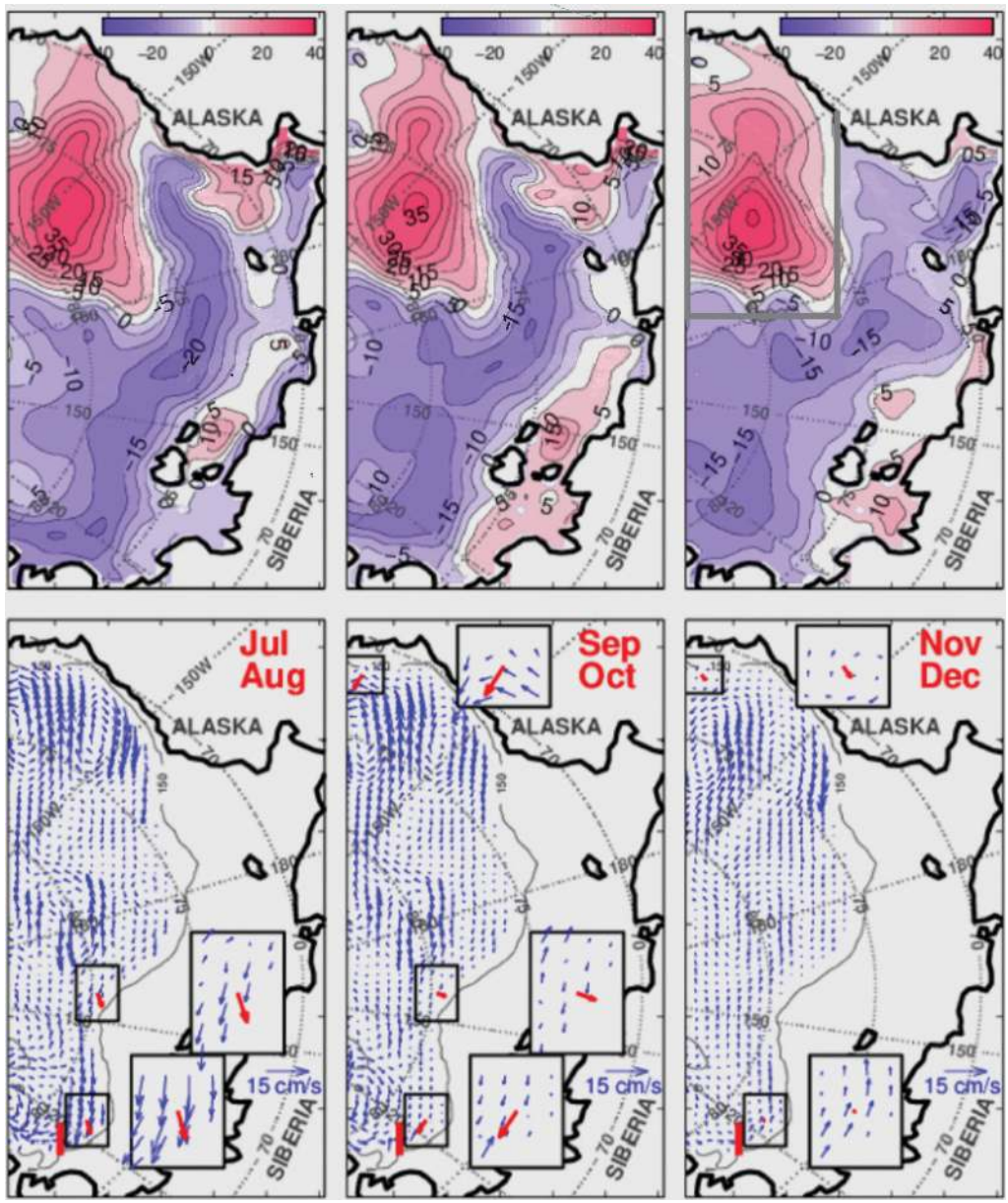

Figure 14.
Bimonthly averaged fields for SSH in cm (upper panels) and velocity at 250 m depth in cm/s (lower panels). NABOS mooring-observed velocities are shown by insets. The boundaries used for calculating the total FW flux around BG are shown by the thick gray line in the top-right panel; the gray line adjacent to the figure panel frame is the "eastern" boundary around BG through which FW transport is positive (gyreward).

the area north of the Bering Strait (upper panels in **Figure 14**), the heights of which are estimated to be −11, −10, and −6 cm, respectively. This is consistent with the seasonal decline of the Bering Strait inflow from 1.1 Sv in July–August to 0.5 Sv in November–December 2008 [20].

The effect of the abovementioned SSH decrease on the transport pattern in the region of the AW inflow is of particular interest. During July–August 2008, the negative SSH anomaly is closely attached to the coastline, creating a positive cross-shelf SSH gradient and a westward geostrophic transport of −2.9 Sv along the shelf break (lower-left panels in **Figure 14**). The effect becomes less visible by the end of the year as the negative SSH anomaly detaches from the continental slope; the total transport relaxes to eastward values of 0.8 and 1.0 Sv, respectively, for the September–October and November–December periods. This identified flow reversal

agrees well with moored velocity observations from the Nansen and Amundsen Basins Observational System (NABOS, http://nabos.iarc.uaf.edu/data), which are indicated by red arrows in **Figure 14** but were not used to obtain the optimized solution.

The DA results immediately provide us with quantitative FWC estimates and permit identification of the regional FW. In particular, the total FWC within the volume bounded within [70.25, 80]°N × [140, 170]°W above 400 m depth was found to be about 20,700 km^3, which is slightly less (∼5%) than that found in literature [update from 46]. A possible source of this difference is a smaller area of the integration for the 4DVar solution and the offshore displacement of the BG observed in 2008.

To assess the FW origin accumulated FWC in the BG, FW transports across the eastern, southern, and western boundaries were estimated 0.08, −0.005, and −0.075 Sv, respectively (positive-oriented gyreward); the boundaries are shown in the top-right panel of **Figure 14**, where the eastern boundary abuts the figure boundary and the southern one intersects the Alaska coast. Calculated transports suggest that observed changes in the BG FWC were generally caused by the FW transport changes confined to the latitude band of 72–77°N at the eastern boundary of the model domain.

6. Summary

This work introduces an IPY snapshot ocean climatology and discusses freshwater and thermal changes in two principle water masses to establish, in perspective, subsurface changes over the central AO as well as consequences of surface freshening. It focuses only on the ocean and readily neglected continental shelves where important water mass-forming processes occur [56] but enhanced mixing impedes analysis based on T/S, any resolvable changes in Arctic Bottom Water, and a direct analysis of sea ice which requires an extensive discussion of the atmosphere and its variability [57] which are beyond the scope of this presentation.

Changes in the AO are not monotonic as they result from cyclic and quasi-cyclic changes in various superimposed feedback-entangled geophysical components in addition to trends in their background values. Changes may arrive in short bursts or "pulses" and may undergo periods of relaxation toward long-term means. The intensive pan-Arctic IPY survey provides evidence of an AO undergoing significant changes and departure from the longer-term mean of the late twentieth century—responding to variations in source content (from the Atlantic, Pacific, and continental waters) and the resulting changes in freshwater and heat distribution; atmospheric forcing, induced SSH gradients, and their associated geostrophic responses; and relative volume and means of exit of various water masses present in the AO. During IPY, many of these components appeared to be establishing new records. In the decade following, 2011–2012 set records for associated components such as river outflow, Bering Strait inflow, sea-ice minimum, and Arctic cyclone strength—some of which may have been surpassed those of 2016–2017. From this perspective, conditions of the AO during IPY 2007–2008 show that the region is in transition toward a "new normal," and a gridded IPY dataset provides a useful reference state for establishing how far that transition has progressed.

A model-DA system was also applied and may quantify the observed difference in the T/S distribution bought on climatological and seasonal temporal scales. The reconstructed mean 2007–2009 AO circulation clearly identified global shifts in the BG and axis of the transpolar drift. Both results are consistent with other qualitative analyses. Analysis of the reconstructed nonstationary circulation for July–December 2008 allowed quantification of several anomalous circulation features including:

a. A reversal of the total transport in the AW inflow region of −2.9 Sv in July–August which later relaxed to an eastward transport of 0.8–1.0 Sv. This reversal of a long-slope current is confirmed by independent observations from NABOS moorings.

b. Formation of a prominent SSH trough extending from the eastern Laptev Sea to the Bering Strait. A similar and even stronger structure was obtained in the PIOMAS solution and is indirectly evidenced by two NABOS moorings located on the continental slope of the Laptev Sea.

c. The aforementioned SSH depression near the Chukchi Sea tends to increase the large-scale sea level difference between the Bering Sea and the AO. This contributes to the 25% increase in the Bering Strait transport at that time and agrees with the regional force balance suggesting an increased role of the pressure head between the Bering Sea and AO during 2007–2011 [20].

d. A significant total FWC of ∼20,700 km^3 in the BG during 2008. The FW accumulation agrees with estimates from in situ hydrographic observations [46]. Analysis of the FW transports across model boundaries around the BG indicates that FW accumulation in 2008 was mainly caused by the anomalous inflow through the eastern section. The DA model estimate of ∼0.8 Sv qualitatively agrees with other works [58, 59] that suggest FW sources may include from near Greenland.

Acknowledgements

J. N. Stroh thanks the University of Nevada, Reno DeLaMare Library, for document preparation resources. G. Panteleev and M. Yaremchuk were supported by the Office of Naval Research (ONR) project "Arctic data assimilation," Program Element 0602435N. O. Francis was supported by the Coastal Hydraulics Engineering Resilience (CHER) Lab, Department of Civil and Environmental Engineering, and National Sea Grant College Program at the University of Hawaii at Manoa. M. Yaremchuk was also supported by the ONR Program Element 0603207N under work on the Navy Earth System Prediction Capability.

Author details

J.N. Stroh[1*], S. Kirillov[2], G. Panteleev[3], O. Francis[4], M. Yaremchuk[3], E. Bloshkina[5] and N. Lebedev[5]

1 Independent Scholar, Fairbanks, AK, USA

2 University of Manitoba, Winnipeg, Canada

3 Naval Research Laboratory, Stennis Space Center, MS, USA

4 University of Hawaii at Manoa, Honolulu, HI, USA

5 Arctic and Antarctic Research Institute, St. Petersburg, Russia

*Address all correspondence to: j.nate.stroh@gmail.com

IntechOpen

References

[1] Rudels B, Jones EP, Anderson LG, Kattner G. On the intermediate depth waters of the Arctic Ocean. In: The polar oceans and their role in shaping the global environment. Washington, D.C.: American Geophyscial Union; 1994. pp. 33-46

[2] Zhang X, Zhang J. Heat and freshwater budgets and pathways in the Arctic Mediterranean in a coupled ocean/sea-ice model. Journal of Oceanography. 2001;**57**(2):207-234

[3] Shiklomanov IA, Shiklomanov AI, Lammers RB, Peterson BJ, Vorosmarty CJ. The dynamics of river water inflow to the Arctic Ocean. In: The Freshwater Budget of the Arctic Ocean. Dordrecht: Springer; 2000. pp. 281-296

[4] Serreze MC, Barrett AP, Slater AG, Woodgate RA, Aagaard K, Lammers RB, et al. The large-scale freshwater cycle of the Arctic. Journal of Geophysical Research: Oceans. 2006;**111**:1-19. C11010

[5] Curry B, Lee CM, Petrie B. Volume, freshwater, and heat fluxes through Davis Strait, 2004–05. Journal of Physical Oceanography. 2011;**41**(3):429-436

[6] Weingartner TJ, Cavalieri DJ, Aagaard K, Sasaki Y. Circulation, dense water formation, and outflow on the northeast Chukchi shelf. Journal of Geophysical Research: Oceans. 1998;**103**(C4):7647-7661

[7] Dmitrenko IA, Rudels B, Kirillov SA, Aksenov YO, Lien VS, Ivanov VV, et al. Atlantic water flow into the Arctic Ocean through the St. Anna trough in the northern Kara Sea. Journal of Geophysical Research: Oceans. 2015; **120**(7):5158-5178

[8] Rudels B, Friedrich HJ, Quadfasel D. The Arctic circumpolar boundary current. Deep Sea Research Part II: Topical Studies in Oceanography. 1999; **46**(6–7):1023-1062

[9] Proshutinsky AY, Johnson MA. Two circulation regimes of the wind-driven Arctic Ocean. Journal of Geophysical Research: Oceans. 1997;**102**(C6): 12493-12514

[10] Woodgate R. Arctic Ocean circulation: Going around at the top of the world. Nature Education Knowledge. 2013;**4**(8):8

[11] Dukhovskoy D, Johnson M, Proshutinsky A. Arctic decadal variability from an idealized atmosphere-ice-ocean model: 2. Simulation of decadal oscillations. Journal of Geophysical Research: Oceans. 2006;**111**:1-17. C06029

[12] Polyakov IV, Johnson MA. Arctic decadal and interdecadal variability. Geophysical Research Letters. 2000; **27**(24):4097-4100

[13] Wang J, Zhang J, Watanabe E, Ikeda M, Mizobata K, Walsh JE, et al. Is the dipole anomaly a major driver to record lows in Arctic summer sea ice extent? Geophysical Research Letters. 2009;**36**(5):1-5. L05706

[14] Shiklomanov AI, Lammers RB. Record Russian river discharge in 2007 and the limits of analysis. Environmental Research Letters. 2009; **4**(4):1-9. 045015

[15] Polyakov IV, Beszczynska A, Carmack EC, Dmitrenko IA, Fahrbach E, Frolov IE, et al. One more step toward a warmer Arctic. Geophysical Research Letters. 2005;**32**(17):1-4. L17605

[16] McPhee MG, Proshutinsky A, Morison JH, Steele M, Alkire MB. Rapid change in freshwater content of the

Arctic Ocean. Geophysical Research Letters. 2009;**36**(10):1-6. L10602

[17] Polyakov IV, Alexeev VA, Ashik IM, Bacon S, Beszczynska-Möller A, Carmack EC, et al. Fate of early 2000s Arctic warm water pulse. Bulletin of the American Meteorological Society. 2011; **92**(5):561-566

[18] Morison J, Kwok R, Peralta-Ferriz C, Alkire M, Rigor I, Andersen R, et al. Changing arctic ocean freshwater pathways. Nature. 2012;**481**(7379):66

[19] Falck E, Kattner G, Budéus G. Disappearance of Pacific water in the northwestern Fram Strait. Geophysical Research Letters. 2005;**32**(14):1-4. L14619

[20] Woodgate RA, Weingartner TJ, Lindsay R. Observed increases in Bering Strait oceanic fluxes from the Pacific to the Arctic from 2001 to 2011 and their impacts on the Arctic Ocean water column. Geophysical Research Letters. 2012;**39**(24):1-6. L24603

[21] Carmack E, McLaughlin F, Yamamoto-Kawai M, Itoh M, Shimada K, Krishfield R, et al. Freshwater storage in the Northern Ocean and the special role of the Beaufort Gyre. In: Arctic–SubArctic Ocean Fluxes. Dordrecht: Springer; 2008. pp. 145-169

[22] Alkire MB, Falkner KK, Rigor I, Steele M, Morison J. The return of Pacific waters to the upper layers of the Central Arctic Ocean. Deep Sea Research Part I: Oceanographic Research Papers. 2007;**54**(9):1509-1529

[23] Zhong W, Zhao J. Deepening of the Atlantic water core in the Canada Basin in 2003–11. Journal of Physical Oceanography. 2014;**44**(9):2353-2369

[24] Steele M, Boyd T. Retreat of the cold halocline layer in the Arctic Ocean. Journal of Geophysical Research: Oceans. 1998;**103**(C5):10419-10435

[25] Emery WJ. Water types and water masses. In: Encyclopedia of Ocean Sciences. Vol. 6. San Diego: Academic Press; 2001. pp. 3179-3187

[26] Stroh JN, Panteleev G, Kirillov S, Makhotin M, Shakhova N. Sea-surface temperature and salinity product comparison against external in situ data in the Arctic Ocean. Journal of Geophysical Research: Oceans. 2015; **120**(11):7223-7236

[27] Steele M, Morley R, Ermold W. PHC: A global ocean hydrography with a high-quality Arctic Ocean. Journal of Climate. 2001;**14**(9):2079-2087

[28] Environmental Working Group. In: Timokhov L, Tanis F, editors. Environmental Working Group Joint U.S.-Russian Atlas of the Arctic Ocean, Version 1. Boulder, Colorado USA: NSIDC: National Snow and Ice Data Center; 1997. DOI: 10.7265/N5H12ZX4. Available from: http://nsidc.org/data/g01961

[29] Francis OP, Yaremchuk M, Panteleev GG, Zhang J, Kulakov M. Anomalous circulation in the Pacific sector of the Arctic Ocean in July–December 2008. Ocean Modelling. 2017; **117**:12-27

[30] Toole JM, Krishfield RA, Timmermans ML, Proshutinsky A. The ice-tethered profiler: Argo of the Arctic. Oceanography. 2011;**24**(3):126-135

[31] Krishfield R, Toole J, Proshutinsky A, Timmermans ML. Automated ice-tethered profilers for seawater observations under pack ice in all seasons. Journal of Atmospheric and Oceanic Technology. 2008;**25**(11): 2091-2105

[32] Troupin C, Barth A, Sirjacobs D, Ouberdous M, Brankart JM, Brasseur P,

et al. Generation of analysis and consistent error fields using the data interpolating variational analysis (DIVA). Ocean Modelling. 2012;**52**: 90-101

[33] Jakobsson M, Mayer L, Coakley B, Dowdeswell JA, Forbes S, Fridman B, et al. The international bathymetric chart of the Arctic Ocean (IBCAO) version 3.0. Geophysical Research Letters. 2012;**39**(12):1-6. L12609

[34] Ekwurzel B, Schlosser P, Mortlock RA, Fairbanks RG, Swift JH. River runoff, sea ice meltwater, and Pacific water distribution and mean residence times in the Arctic Ocean. Journal of Geophysical Research: Oceans. 2001; **106**(C5):9075-9092

[35] Steele M, Morison J, Ermold W, Rigor I, Ortmeyer M, Shimada K. Circulation of summer Pacific halocline water in the Arctic Ocean. Journal of Geophysical Research: Oceans. 2004; **109**:1-18. C02027

[36] Shimada K, Itoh M, Nishino S, McLaughlin F, Carmack E, Proshutinsky A. Halocline structure in the Canada Basin of the Arctic Ocean. Geophysical Research Letters. 2005;**32**(3):1-5. L03605

[37] Shimada K, Carmack EC, Hatakeyama K, Takizawa T. Varieties of shallow temperature maximum waters in the western Canadian Basin of the Arctic Ocean. Geophysical Research Letters. 2001;**28**(18):3441-3444

[38] Bourgain P, Gascard JC. The Atlantic and summer Pacific waters variability in the Arctic Ocean from 1997 to 2008. Geophysical Research Letters. 2012;**39**(5):1-6. L05603

[39] McLaughlin FA, Carmack EC, Williams WJ, Zimmermann S, Shimada K, Itoh M. Joint effects of boundary currents and thermohaline intrusions on the warming of Atlantic water in the Canada Basin, 1993–2007. Journal of Geophysical Research: Oceans. 2009; **114**:1-20. C00A12

[40] Polyakov IV, Timokhov LA, Alexeev VA, Bacon S, Dmitrenko IA, Fortier L, et al. Arctic Ocean warming contributes to reduced polar ice cap. Journal of Physical Oceanography. 2010; **40**(12):2743-2756

[41] Morison J, Steele M, Kikuchi T, Falkner K, Smethie W. Relaxation of Central Arctic Ocean hydrography to pre-1990s climatology. Geophysical Research Letters. 2006;**33**(17):1-5. L17604

[42] Rabe B, Karcher M, Schauer U, Toole JM, Krishfield RA, Pisarev S, et al. An assessment of Arctic Ocean freshwater content changes from the 1990s to the 2006–2008 period. Deep Sea Research Part I: Oceanographic Research Papers. 2011;**58**(2):173-185

[43] Ge S, Yang D, Kane DL. Yukon River basin long-term (1977–2006) hydrologic and climatic analysis. Hydrological Processes. 2013;**27**(17): 2475-2484

[44] Zhang T, Frauenfeld OW, Serreze MC, Etringer A, Oelke C, McCreight J, et al. Spatial and temporal variability in active layer thickness over the Russian Arctic drainage basin. Journal of Geophysical Research: Atmospheres. 2005;**110**:1-14. D16101

[45] Shiklomanov AI, Lammers RB, Rawlins MA, Smith LC, Pavelsky TM. Temporal and spatial variations in maximum river discharge from a new Russian data set. Journal of Geophysical Research: Biogeosciences. 2007;**112**:1-14. G04S53

[46] Proshutinsky A, Krishfield R, Timmermans ML, Toole J, Carmack E, McLaughlin F, et al. Beaufort Gyre

freshwater reservoir: State and variability from observations. Journal of Geophysical Research: Oceans. 2009; **114**:1-25. C00A10

[47] De Steur L, Steele M, Hansen E, Morison J, Polyakov I, Olsen SM, et al. Hydrographic changes in the Lincoln Sea in the Arctic Ocean with focus on an upper ocean freshwater anomaly between 2007 and 2010. Journal of Geophysical Research: Oceans. 2013; **118**(9):4699-4715

[48] Curry B, Lee CM, Petrie B, Moritz RE, Kwok R. Multiyear volume, liquid freshwater, and sea ice transports through Davis Strait, 2004–10. Journal of Physical Oceanography. 2014;**44**(4): 1244-1266

[49] Beszczynska-Möller A, Woodgate RA, Lee C, Melling H, Karcher M. A synthesis of exchanges through the main oceanic gateways to the Arctic Ocean. Oceanography. 2011;**24**(3):82-99

[50] McPhee MG. Intensification of geostrophic currents in the Canada Basin, Arctic Ocean. Journal of Climate. 2013;**26**(10):3130-3138

[51] Armitage TW, Bacon S, Kwok R. Arctic Sea level and surface circulation response to the Arctic oscillation. Geophysical Research Letters. 2018;**45**: 6576-6584

[52] Panteleev G, Yaremchuk M, Stabeno PJ, Luchin V, Nechaev DA, Kikuchi T. Dynamic topography of the Bering Sea. Journal of Geophysical Research: Oceans. 2011;**116**:1-11. C05017

[53] Luchin V, Panteleev G. Thermal regimes in the Chukchi Sea from 1941 to 2008. Deep Sea Research Part II: Topical Studies in Oceanography. 2014;**109**: 14-26

[54] Panteleev G, Nechaev DA, Proshutinsky A, Woodgate R, Zhang J. Reconstruction and analysis of the Chukchi Sea circulation in 1990–1991. Journal of Geophysical Research: Oceans. 2010;**115**:1-22. C08023

[55] Timmermans ML, Proshutinsky A, Krishfield RA, Perovich DK, Richter-Menge JA, Stanton TP, et al. Surface freshening in the Arctic Ocean's Eurasian Basin: An apparent consequence of recent change in the wind-driven circulation. Journal of Geophysical Research: Oceans. 2011;**116**: 1-17. C00D03

[56] Semiletov I, Dudarev O, Luchin V, Charkin A, Shin KH, Tanaka N. The east Siberian Sea as a transition zone between Pacific-derived waters and Arctic shelf waters. Geophysical Research Letters. 2005;**32**(10):1-5. L10614

[57] Maslanik J, Drobot S, Fowler C, Emery W, Barry R. On the Arctic climate paradox and the continuing role of atmospheric circulation in affecting sea ice conditions. Geophysical Research Letters. 2007;**34**(3):1-4. L03711

[58] Lique C, Garric G, Treguier AM, Barnier B, Ferry N, Testut CE, et al. Evolution of the Arctic Ocean salinity, 2007–08: Contrast between the Canadian and the Eurasian basins. Journal of Climate. 2011;**24**(6): 1705-1717

[59] Proshutinsky A, Dukhovskoy D, Timmermans ML, Krishfield R, Bamber JL. Arctic circulation regimes. Philosophical Transactions of the Royal Society A. 2015;**373**(2052):1-18. 20140160